Anomalous structure in the single particle spectrum of the fractional quantum Hall effect

O. E. Dial[*], R. C. Ashoori[*], L. N. Pfeiffer[†], K. W. West[†]

May 24, 2010

Abstract

The two-dimensional electron system (2DES) is a unique laboratory for the physics of interacting particles. Application of a large magnetic field produces massively degenerate quantum levels known as Landau levels. Within a Landau level the kinetic energy of the electrons is suppressed, and electron-electron interactions set the only energy scale[1]. Coulomb interactions break the degeneracy of the Landau levels and can cause the electrons to order into complex ground states. In the high energy single particle spectrum of this system, we observe salient and unexpected structure that extends across a wide range of Landau level filling fractions. The structure appears only when the 2DES is cooled to very low temperature, indicating that it arises from delicate ground state correlations. We characterize this structure by its evolution with changing electron density and applied magnetic field. We present two possible models for understanding these observations. Some of the energies of the features agree qualitatively with what might be expected for composite Fermions, which have proven effective for interpreting other experiments in this regime. At the same time, a simple model with electrons localized on ordered lattice sites also generates structure similar to those observed in the experiment. Neither of these models alone is sufficient to explain the observations across the entire range of densities measured. The discovery of this unexpected prominent structure in the single particle spectrum of an otherwise thoroughly studied system suggests that there exist core features of the 2DES that have yet to be understood.

Our measurements are performed using time domain capacitance spectroscopy (TDCS)[2;3], which allows measurement of the single particle density of states (SPDOS) with accurately calibrated energy and density scales. The technique uses a repeated series of electronic pulses to measure I/V tunnelling characteristics,

[*]Massachusetts Institute of Technology, Cambridge, MA 02139, USA

[†]Alcatel-Lucent Bell Laboratories, Murray Hill, New Jersey 07974, USA (present address: Princeton, Princeton New Jersey, 08544, USA.

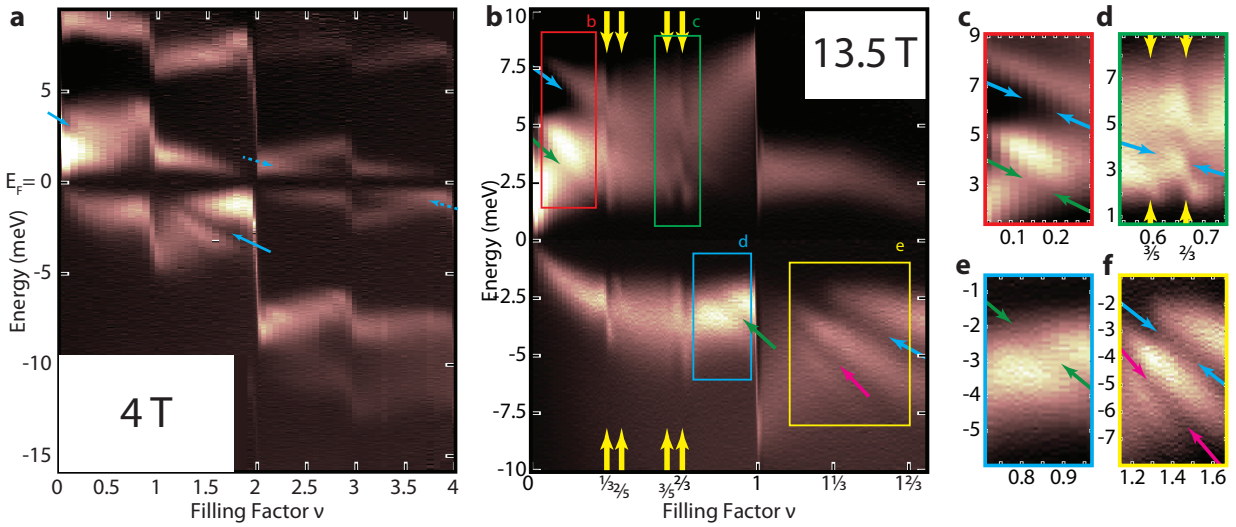

Figure 1: **High field TDCS spectra show "sash" features: bright and dark diagonal lines across the spectrum.** The horizontal axis in each spectrum is the electron density in the quantum well, expressed as a filling factor ν with $\nu = 1$ corresponding to completely filling the lowest spin-polarized Landau level. The vertical axis is energy measured from E_f, with $E > 0$ corresponding to injecting electrons into empty states in the quantum well and $E < 0$ corresponding to ejecting electrons from filled states. Bright regions correspond to high SPDOS. In the spectrum taken at a temperature of 100 mK with a 4 Tesla perpendicular magnetic field shown in **a**, features associated with the $\nu = 1$ sash are highlighted with a blue arrow, while another sash about $\nu = 3$ is indicated with a dashed blue arrow. In the 13.5 Tesla data in **b**, taken at 80 mK, the $\nu = 1$ sash is similarly indicated with blue arrows, while the $\nu = 1/2$ sash about $\nu = 1/2$ is indicated with green. Sharp downward steps in the spectrum corresponding to chemical potential jumps at filling fractions corresponding to fractional quantum Hall plateaus are indicated with yellow arrows. The contrast for positive and negative energies has been adjusted separately in this spectrum. **c-f**, selected regions of the spectrum are blown up and their contrast enhanced to ease identification of the features, indicated with arrows that match the colors in **b**.

with delays between the pulses to allow the sample to re-equilibrate. Two experimental enhancements make the results described in this letter possible. First, compared to our previous work, we use a sample with a wider, 230Å quantum well to confine the electrons in two-dimensions. This reduces the scattering from fluctuations in the well thickness[4]. Secondly, we have enhanced our experimental technique to allow us to measure spectra at higher magnetic fields (see supplement). The spacing between Landau level orbit centers is smaller at higher fields, increasing the energy scale of the Coulomb interaction and separating features more clearly in the spectrum.

As described in our previous work[3], as we vary the filling factor from $\nu = 0$ to 1 the inter-electron spacing decreases. This causes an increased Coulomb interaction that opens an exchange gap between spin-up and spin-down states at the Fermi surface. Generically, we then expect to see one peak above the Fermi energy E_f ($E = 0$ in our plots), and one peak below E_f in the SPDOS, and those peaks should move away from each-other as we raise the density. Similarly, we expect to see exchange gaps collapse as we raise the density in the $1 < \nu < 2$ range, so the two peaks will approach E_f again as we raise the density to $\nu = 2$.

At higher magnetic fields, several new features become apparent that are not explained within this simple exchange-based framework.

At a perpendicular magnetic field B of 4 Tesla, an additional tunneling feature (the edge of this feature closest to E_f is delineated with blue arrows in Figure 1**a**) appears at roughly 4 meV near zero density, with an energy that decreases towards $E = 0$ as it approaches $\nu = 1$. This trend with density is surprising; this is a region where we expect to see the exchange gap opening, and states correspondingly moving away from the Fermi energy. A second feature that appears to be a continuation of this line extends towards increasingly negative energies between $\nu = 1$ and 2, once again moving counter to the behaviour of the exchange gap. We will refer to these features as the "$\nu = 1$ sash". Near $E = 0$, we see a dark band of suppressed tunnelling caused by the magnetic field induced Coulomb gap[2;5–8].

On increasing B to 13.5 Tesla (Figure 1**b-f**), we find this $\nu = 1$ sash (blue arrows) becomes more distinct and shifts to higher energies. In addition, we see "jumps" in our data at $\nu = 1/3$, 2/5, 3/5, and 2/3 (yellow arrows). These result from chemical potential variations at the fractional quantum Hall (FQH) plateaus, as observed elsewhere[9;10]. A second "$\nu = 1/2$" sash also becomes visible at smaller energies, extrapolating to zero energy at $\nu = 1/2$ (green arrows). An additional sash also appears below the $\nu = 1$ sash, in the vicinity of $1 < \nu < 2$ (purple arrow).

These sashes are destroyed at 13.5 Tesla when we raise the sample temperature to 4 K, while the exchange splitting and integer quantum Hall features survive (see supplemental figure 1). Despite their high energies in the spectrum (up to 8 meV), a relatively small thermal energy of 0.4 meV suffices to eliminate these sashes. This demonstrates a remarkable property of the single particle spectrum: the high energy spectral features depend on fragile properties of the 2DES that only develop at low temperatures.

All of these sashes have the opposite density dependence than that expected from the opening and closing of the exchange gap, show a linear dependence in energy on filling fraction which becomes steeper as B is raised, and appear to cross the Fermi energy close to either $\nu = 1$ or $\nu = 1/2$. These similarities suggest that we may be able to explain all these additional features using a single underlying origin. The asymmetry of the sashes about the Fermi energy rules out inelastic tunnelling as a possible origin. Their appearance in quantum wells in several different heterostructures excludes defect-induced resonances in the tunnelling barrier.

One hypothesis, suggested by the location of the $\nu = 1$ sash, would be the identification of the quasi-particles as "skyrmions," a coupled spin-charge excitation known to be important near $\nu = 1$[11]. Although skyrmions exist as part of the ground state only near $\nu = 1$[12–14], they may exist as high-energy excitations away from $\nu = 1$ where the sash is visible. However, the energy and existence of skyrmions is sensitive to the total magnetic field, not only the perpendicular magnetic field[13]. Measurements with tilted magnetic fields

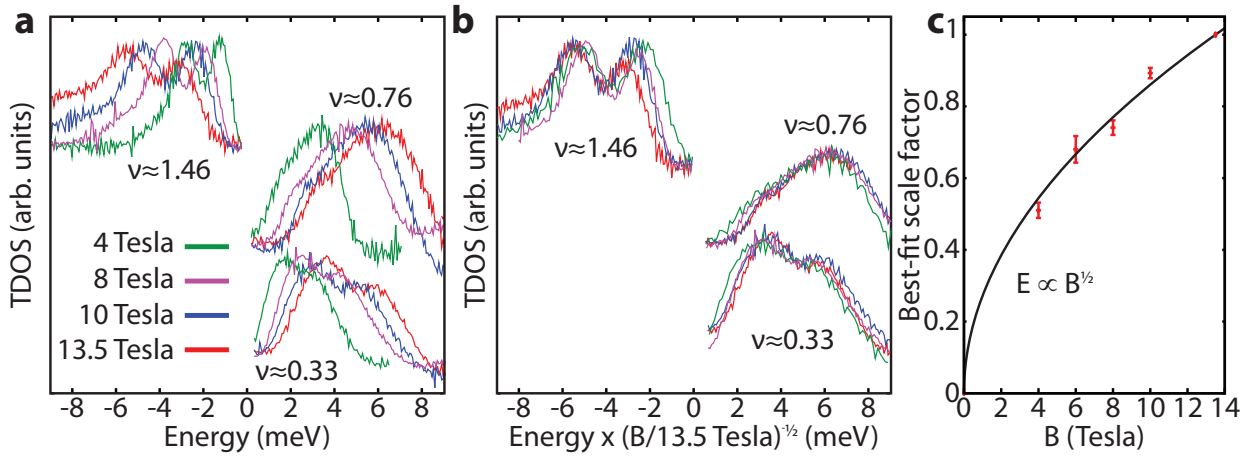

Figure 2: **A $\sqrt{B}$ energy dependence indicates the sashes originate with electron-electron interactions within the lowest Landau levels**. Linecuts at several magnetic fields, all at 100 mK, and at a variety of filling factors are plotted in **a**, showing a number of peaks owing to the unexpected sashes. In **b**, the energy (horizontal) axis has been scaled by $1/\sqrt{B}$, collapsing the peaks associated with the $\nu = 1/2$ and $\nu = 1$ sashes. Residual mismatch in the peak locations is predominantly due to small mismatches in the filling fraction selected at each magnetic fields. Best-fit scaling factors averaged across all densities for each magnetic field are shown in **c**, with a square-root dependence on B shown for reference. Error bars indicate the sample standard deviation for the best-fit scaling factor as a function of density. For fitting details and alternate functional dependences see supplement.

do not reveal any change in the energy of the sash (See suppl. figure 2). Furthermore, the presence of a second sash (purple arrow in Figure 1**b**) in the fan of features at $\nu > 1$ is inconsistent with this interpretation.

In the absence of a model for the lineshape of these new features, it is difficult to extract their exact energies to study their dependence on magnetic field. However, just as we can identify the linear dependence of the "sash" energies with density by examining their evolution with filling fraction at fixed magnetic field, we can also make precise comparisons between spectra at different B but similar ν (Figure 2**a**). We find an energy scaling factor that depends only on B can be used to collapse all of the peaks in each spectrum onto the 13.5 Tesla spectrum (Figure 2**b**). This scaling factor grows as $\sqrt{B}$ (Figure 2**c**). The only fundamental energy scale in this system with this magnetic field dependence is the Coulomb energy scale, proportional to the inverse inter-electron separation. This $\sqrt{B}$ scaling indicates that it may be possible to interpret the new "sash" features in terms of composite Fermions, weakly interacting quasiparticles whose properties are determined entirely by electron-electron interactions.

One interpretation of the paired nature of our sashes above and below the Fermi energy is that they are part of a single, continuous excitation that projects through the Fermi energy, with the region near zero energy obscured by the Coulomb gap. The $\nu = 1/2$ sash then extrapolates through E_f at $\nu = 1/2$ (green arrows in Figure 1**b,c,e**) Composite Fermions with two attached flux quanta (^{2}CFs) experience an effective magnetic field $B^* = B(1 - 2\nu)$. If we imagine sweeping the density in the 2DES while injecting a probe

^{2}CF the ^{2}CF will experience zero magnetic field at $\nu = 1/2$, with an effective magnetic field that increases as one moves away from $\nu = 1/2$ (red line in Figure 3a). A Landau fan of ^{2}CFs would then follow the same trend in energy that we see in our $\nu = 1/2$ sash (Figure 3**c**). We measure our spectra relative to the Fermi energy, which is the same for composite fermions and electrons[15]; shifting the Landau fan to place E_f at $E = 0$ yields the fan in Figure 3**d**. Note the whole electron may not be able to directly break up into composite Fermions; if the CF interpretation is correct, the features in our spectrum are clouds of incoherent excitations whose lower energy edge is the true CF energy (see supplement).

For $\nu < 1/3$, the ^{2}CF filling factor ν^* is less than 1 (Figure 3**b**); this means that there are no quasi-Landau levels below the Fermi energy, and we only expect to see states at $E > 0$. However, for $\nu > 2/3$, ν^* is between one and two; the model predicts a single quasi-Landau level below the Fermi energy. Examination of the fan in Figure 3**e,f** clearly shows this expected asymmetry. We find that we can observe this sash over a wide variety of filling fractions, including those corresponding to FQH plateaus caused by other quasiparticles. This is consistent with prior experiments[16] and theoretical work[17]. We do not observe ^{2}CF Landau levels that would correspond to $n^* \geq 2$ in these spectra. In the regions where we observe ^{2}CF Landau levels, these would be high energy excitations that should not be well described by composite Fermion theory and may not even exist. Unsurprisingly, we do not observe ^{2}CF states near $\nu = 1/2$ where they would be expected to fall inside of the Coulomb gap.

In this interpretation, the slopes of the lines in our Landau fans $dE/d\nu$ relate directly to the quasiparticle effective masses; for each ^{2}CF splitting, $E = \pm\hbar eB(1-2\nu)/m^*$, so $dE/d\nu = \pm\hbar e2B/m^*$. Using this relation we estimate a mass of $(0.35 \pm 0.06)m_0$, where m_0 is the free electron mass, for the ^{2}CF at 13.5 Tesla magnetic field. Theoretical estimates of the width of the gap at 13.5 Tesla give typical values of m^*/m_0 of 0.23[18] or 0.31[15]. Finite well width effects will increase these masses slightly[19]. The aforementioned $\sqrt{B}$ dependence of the sash features yields a $\sqrt{B}$ dependence of the cyclotron mass, as is predicted and as has been observed in thermally activated transport measurements[20]. The observed Landau gap for the $\nu = 1/2$ sash is roughly a factor of four larger than that reported from thermally activated conductivity, and the mass is correspondingly smaller[20]. However, similar discrepancies in measurements of the exchange gap suggest that thermal activation measurements may underestimate the widths of gaps at the Fermi energy[3].

The $\nu = 1$ sash features do not afford a simple explanation in terms of composite Fermions; extending the model to other composite quasiparticles with p vortices attached allows us to explain any "sashes" which intersect the Fermi energy at a filling factors $\nu = 1/p$ where p is even[21]. For a fully spin polarized excitation, $p = 1$ would correspond to an excitation which has the wrong symmetry under exchange to be an electron wavefunction. However, the $\nu = 1$ sash features form a "fan" of states with evenly spaced energies (Figure 4**a**), suggesting it may be possible to explain them in terms of injecting electrons into states that

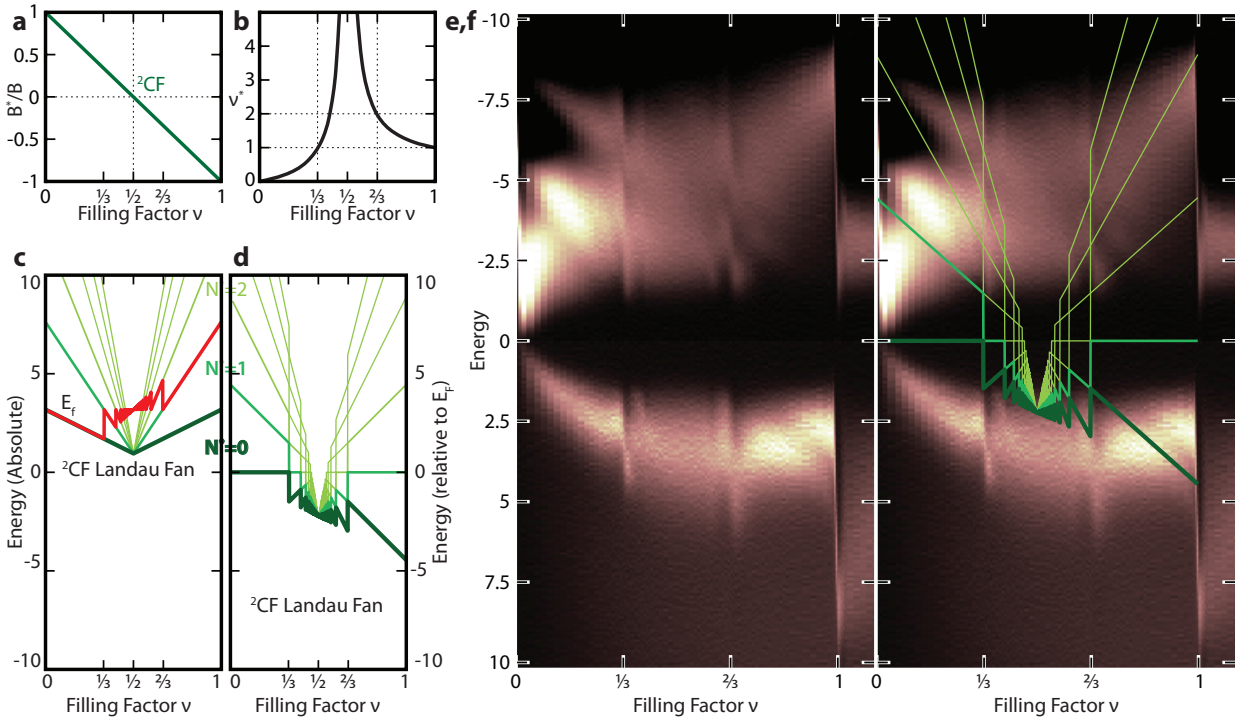

Figure 3: **From the viewpoint of a composite quasiparticle, sweeping the density in a quantum well also sweeps the effective magnetic field.** Panel **a** shows the effective field experienced by a ^{2}CF as the electron density is swept through the first Landau level. As the effective field and particle density are swept, the filling factor of ^{2}CF composite fermions $\nu^* = \nu/(1-2\nu)$ changes (**b**). In **c**, a Landau fan, simplified by assuming a constant CF effective mass, $E = \hbar\omega_c(n+1/2)$ for the ^{2}CF is shown in absolute energy, with the Fermi energy shown in red: $E_f = \hbar\omega_c(n_f+1/2)$, with n_f the greatest integer less than ν^* ($n_f = \lfloor \nu^* \rfloor$). The Fermi energy rises as the ^{2}CF density increases in the quantum well. In **d**, the fan is shifted to place E_f at $E=0$, showing the fan as it is expected to appear in TDCS spectra. The 13.5 Tesla TDCS spectrum without (**e**) and with (**f**) the fan superimposed allows identification of the two $\nu = 1/2$ sash features with a Landau level of the ^{2}CF fan closest to the Fermi surface. Lines suggested by the fan but not observed have been included to show alignment with chemical potential jumps associated with known FQH states, as well as to demonstrate the origin of the asymmetry when high energy CF Landau levels (lightest lines) are not observed.

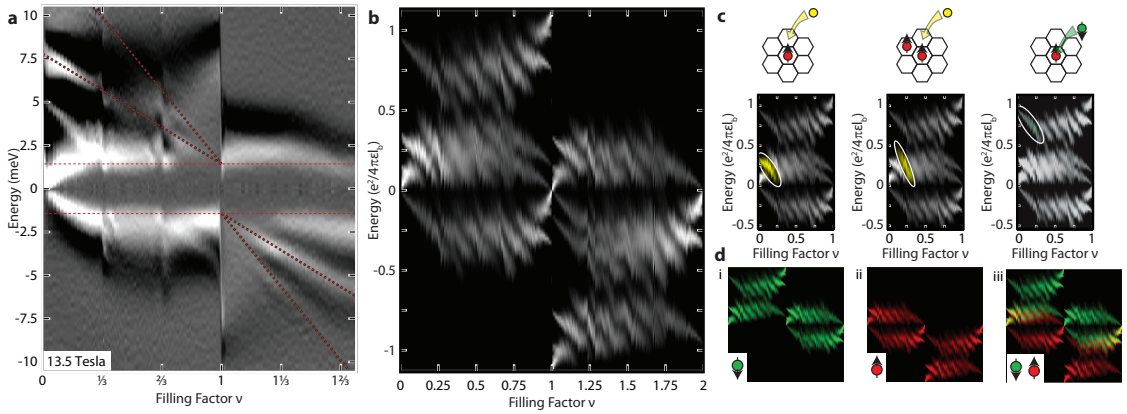

Figure 4: **The $\nu = 1$ sash features can be emphasized by taking an additional derivative of the data, easing comparison to simulated spectra from a model of electrons localized on a lattice.** Panel **a** shows the wide range of fractions over which the $\nu = 1$ sash persists. Noise introduced in the image by taking the second derivative has been diminished by smoothing with a $\sigma = 160\mu$eV Gaussian. The onset energies of the "clouds" of excitations are evenly spaced in energy, allowing a simple fan to describe all of the excitations. In **b**, a sample spectrum from the lattice model is shown. The right axis is in units of $e^2/(4\pi\epsilon l_b)$, roughly 16 meV at 13.5 Tesla. The "sashes" that move downward in energy as the density is raised originate with different types of sites that can be populated or depopulated. The origins of selected prominent features are indicated with cartoons of the relevant lattice situations in **c**. Each cartoon is accompanied by a replica of the spectrum for $0 < \nu < 1$ with the relevant portion highlighted. The hexagons represent lattice cells of a hexagonal lattice, with single particle states in the center of each hexagon. Tunneling an electron of either spin (yellow) onto a site adjacent to an occupied site (i) may give rise to our $\nu = 1/2$ sash, the lowest energy sash at low densities. A similar sash occurs at slightly higher densities (ii) corresponding to tunneling an electron onto a site adjacent to two occupied sites. Tunneling a minority spin (green) electron onto a site already occupied by a majority spin (red) electron (iii) appears to give rise to our $\nu = 1$ sash, the highest energy sash at low densities. For reference, a breakdown of the spectrum by spin is provided in **d**, with the minority spins only (i), the majority spins only (ii), and the majority and minority spin states color coded. Note that the minority carriers in the lowest Landau level are always completely spin polarized in this model if the on-site repulsion is larger than the peak-to-peak disorder amplitude.

experience a density dependent effective magnetic field.

The theory of composite Fermions makes an ansatz to identify weakly interacting quasiparticles that give rise to the fractional quantum Hall effect. It is expected to accurately capture the low energy physics near $\nu = 1/2$. Given that our observations are at quite large energies and far from $\nu = 1/2$, it is remarkable that this identification appears consistent with our results. Despite this, it is worth noting that inelastic light scattering measurements of for $1/5 < \nu < 1/3$ measure collective excitations of composite Fermions at energies which, when adjusted for well width and magnetic field, are comparable to our ^{2}CF energies[16].

With these concerns in mind, we note the sashes persists down to very low densities where it seems likely a semiclassical description is possible. One very simple model is that described by Fogler et al[22]; consider a hexagonal lattice of sites, each of which has an occupation number for each electron spin $n_i^{\uparrow\downarrow}$ equal to zero or one (each site can have zero, one, or two electrons) and uncorrelated Gaussian distributed disorder potential. The inter-site separation is selected such that the lattice is completely filled at $\nu = 1$. The electrons interact through a repulsive effective potential that includes screening from the tunnel electrode, while electrons of the same spin experience an additional very short range attractive exchange potential. For each density, the total energy is minimized by rearranging the electrons and the excited state spectrum is calculated (see supplement for details).

In the resulting spectra (figure Figure 4**b**), we see, as expected, the development of an exchange splitting as the total density approaches $\nu = 1$[23] as well as a Coloumb gap at zero energy[24]. The calculated exchange splitting is much larger than the observed, possibly due to the aforementioned finite well width effects. Several additional bands of states emerge that are reminiscent of the sashes in our spectra. These bands are insensitive to the exact heterostructure: screening by the tunneling electrode is unimportant. Near zero density, the lattice is populated by a small number of spin up (majority spin) electrons located at minima in the disorder potential. The highest energy "sash" here corresponds to putting a spin down (minority spin) electron onto a site that has already been occupied by a spin up electron; it is displaced upwards in energy by roughly $e^2/(4\pi\epsilon l_b)$ by the on-site Coulomb repulsion. The next highest energry "sash" corresponds to putting either spin electron onto a site that neighbors an occupied site. These bands have a similar structure to the experimentally observed $\nu = 1$ and $\nu = 1/2$ sashes respectively. The energies of these features decrease as the density is raised because the Fermi energy, the energy required to add an electron to the system after allowing the system to relax, is increasing; as the system is filled, new electrons are forced to be placed closer to their nearest neighbors. Eventually, the type of site associated with each sash will become the lowest energy type of site left to fill, causing the sash to merge with the Coulomb gap. For example, the sash associated with diagram (i) in Figure 4**c** merges with the Fermi energy at $\nu = 1/4$. The sash originating with diagram (iii) is more complicated. At low densities, this sash corresponds to injecting a

minority spin electron into already occupied lattice sites. However, near $\nu = 1$, the simulated sash's physical origin has changed, now corresponding to adding an up or down spin electron on top of a site that has not been occupied. This suggests that at low densities the $\nu = 1$ sash is an electrostatically unfavorable excitation involving a spin-singlet composed of the injected electron and an electron already present in the 2DES. Additional features in the simulation not seen in our measurements correspond to clusters of more than two electrons and are probably an artifact of the lattice onto which we have forced the electrons.

We expect this lattice model to be a fair description near $\nu = 0$ and $\nu = 1$ where the 2DEG can be described as a Wigner lattice of disorder pinned electrons (making our initial choice of localized single particle states accurate). The main physics the model then brings to light is the emergence of several discrete high energy bands due to quantization of the electron separations at short distances. However, even in these regimes we note that all of the sashes in the calculation have the same slope, while several distinct slopes are present in the experimental data. The lattice model should become increasingly inaccurate at the intermediate densities where the artificial localization of the electronic states will fail. Here, the composite Fermion model may be more appropriate. Both models predict similar features at the same energies and agree roughly with our experimental spectra but also predict features that do not appear in our spectrum. It is unclear if these two views each have a distinct realm of validity or if they are equivalent in some range of energies and densities in the sense of approximately describing the same physics.

Whatever the precise explanation for the sashes, their existence and prominence in a fundamental spectrum of a system otherwise so thoroughly studied comes a stunning surprise. A detailed and accurate explanation of this spectrum will provide key insights into our microscopic understanding of the ground state of a 2D electronic system.

References

[1] Jain, J. K. *Composite fermions* (Cambridge University Press, 2007).

[2] Chan, H. B., Glicofridis, P. I., Ashoori, R. C. & Melloch, M. R. Universal linear density of states for tunneling into the two-dimensional electron gas in a magnetic field. *Phys. Rev. Lett.* **79**, 2867–2870 (1997).

[3] Dial, O. E., Ashoori, R. C., Pfeiffer, L. N. & West, K. W. High-resolution spectroscopy of two-dimensional electron systems. *Nature* **448**, 176–179 (2007).

[4] Luhman, D. R., Tsui, D. C., Pfeiffer, L. N. & West, K. W. Electronic transport studies of a systematic series of GaAs/AlGaAs quantum wells. *Appl. Phys. Lett.* **91**, 072104 (2007).

[5] Ashoori, R. C., Lebens, J. A., Bigelow, N. P. & Silsbee, R. H. Equilibrium tunneling from the 2-dimensional electron-gas in GaAs - evidence for a magnetic-field-induced energy-gap. *Phys. Rev. Lett.* **64**, 681–684 (1990).

[6] Eisenstein, J. P., Pfeiffer, L. N. & West, K. W. Coulomb barrier to tunneling between parallel two-dimensional electron systems. *Phys. Rev. Lett.* **69**, 3804–3807 (1992).

[7] Ashoori, R. C., Lebens, J. A., Bigelow, N. P. & Silsbee, R. H. Energy gaps of the two-dimensional electron gas explored with equilibrium tunneling spectroscopy. *Phys. Rev. B* **48**, 4616–4628 (1993).

[8] Yang, S.-R. E. & MacDonald, A. H. Coulomb gaps in a strong magnetic field. *Phys. Rev. Lett.* **70**, 4110–4113 (1993).

[9] Eisenstein, J. P., Pfeiffer, L. N. & West, K. W. Compressibility of the two-dimensional electron gas: Measurements of the zero-field exchange energy and fractional quantum Hall gap. *Phys. Rev. B* **50**, 1760–1778 (1994).

[10] Khrapai, V. S. *et al.* Direct measurements of fractional quantum Hall effect gaps. *Phys. Rev. Lett.* **99**, 086802 (2007).

[11] Sondhi, S. L., Karlhede, A., Kivelson, S. A. & Rezayi, E. H. Skyrmions and the crossover from the integer to fractional quantum Hall effect at small Zeeman energies. *Phys. Rev. B* **47**, 16419–16426 (1993).

[12] Barrett, S. E., Dabbagh, G., Pfeiffer, L. N., West, K. W. & Tycko, R. Optically pumped NMR evidence for finite-size skyrmions in GaAs quantum wells near Landau level filling $\nu = 1$. *Phys. Rev. Lett.* **74**, 5112–5115 (1995).

[13] Schmeller, A., Eisenstein, J. P., Pfeiffer, L. N. & West, K. W. Evidence for skyrmions and single spin flips in the integer quantized Hall effect. *Phys. Rev. Lett.* **75**, 4290–4293 (1995).

[14] Gallais, Y., Yan, J., Pinczuk, A., Pfeiffer, L. N. & West, K. W. Soft spin wave near $nu = 1$: Evidence for a magnetic instability in skyrmion systems. *Phys. Rev. Lett.* **100**, 086806 (2008).

[15] Halperin, B. I., Lee, P. A. & Read, N. Theory of the half-filled Landau level. *Phys. Rev. B* **47**, 7312–7343 (1993).

[16] Hirjibehedin, C. F., Pinczuk, A., Dennis, B. S., Pfeiffer, L. N. & West, K. W. Crossover and coexistence of quasiparticle excitations in the fractional quantum Hall regime at $\nu \leq 1/3$. *Phys. Rev. Lett.* **91**, 186802 (2003).

[17] Peterson, M. R. & Jain, J. K. Flavor altering excitations of composite fermions. *Phys. Rev. Lett.* **93**, 046402 (2004).

[18] Morf, R. & d'Ambrumenil, N. Stability and effective masses of composite fermions in the first and second Landau level. *Phys. Rev. Lett.* **74**, 5116–5119 (1995).

[19] Park, K., Meskini, N. & Jain, J. K. Activation gaps for the fractional quantum Hall effect: realistic treatment of transverse thickness. *Journal of Physics: Condensed Matter* **11**, 7283–7299 (1999).

[20] Leadley, D. R., van der Burgt, M., Nicholas, R. J., Foxon, C. T. & Harris, J. J. Pulsed-magnetic-field measurements of the composite-fermion effective mass. *Phys. Rev. B* **53**, 2057–2063 (1996).

[21] Jain, J. K. Composite-fermion approach for the fractional quantum Hall effect. *Phys. Rev. Lett.* **63**, 199–202 (1989).

[22] Fogler, M. M., Koulakov, A. A. & Shklovskii, B. I. Ground state of a two-dimensional electron liquid in a weak magnetic field. *Phys. Rev. B* **54**, 1853–1871 (1996).

[23] Ando, T. & Uemura, Y. Theory of oscillatory g factor in an MOS inversion layer under strong magnetic fields. *J. Phys. Soc. Jpn.* **37**, 1044–1052 (1974).

[24] Pikus, F. G. & Efros, A. L. Coulomb gap in a two-dimensional electron gas with a close metallic electrode. *Phys. Rev. B* **51**, 16871–16877 (1995).

Supplementary Information is linked to the online version of the paper at www.nature.com/nature.

Acknowledgments We are grateful to Alan MacDonald and Yigal Meir, who independently suggested the identification of sash features with nearby localized states that formed the basis for the lattice model. We thank Patrick Lee, Leonid Levitov and Bert Halperin for helpful discussions regarding the interpretation of our results. This work was sponsored by the Office of Science, Basic Energy Sciences, of the US Department of Energy.

Author Contributions O.E.D. built the apparatus and performed measurements and analysis. R.C.A. supervised the work and performed analysis. O.E.D. and R.C.A. prepared the manuscript. L.N.P. and K.W.W. performed the crystal growth.

Author Information Reprints and permissions information is available at www.nature.com/reprints. Correspondence and requests for materials should be addressed to O.E.D. (dial@alum.mit.edu) or R.C.A. (ashoori@mit.edu).

Supplementary Material

1 Discharge Pulses

Previous measurements were limited to low magnetic fields because of the magnetic field induced coulomb gap at the Fermi energy[3,5–8]; vanishing tunnel current near equilibrium caused the re-equilibration time to grow rapidly with increasing magnetic field, making the measurement impractical.

We have extended the technique to include a "discharge pulse", a brief pulse of the opposite polarity of the pulse used to measure the tunnel current, whose width is tuned to remove exactly the amount of charge that tunneled in during the application of the measurement pulse. This rapidly returns the device to near-equilibrium. The tuning is performed by monitoring the tunneling current for several tens of microseconds (this time is increased as the magnetic field is increased) after the discharge pulse to insure that the sample is re-equilibrated. This time period also allows the 2DES to re-thermalize. We confirm that this re-thermalization is complete by varying the delay between pulse repetitions and confirming that we measure the same I/V curve.

2 Energy Scaling

The energy scaling factor for each magnetic field shown in Figure 2 of the main text was determined by maximizing the correlation between d^2I/dV^2 spectra taken at the same density but at two different magnetic fields. First, for each filling in the higher field spectrum, the closest filling factor in the lower field spectrum is selected. Then, the spectra are numerically differentiated a second time, giving d^2I/dV^2; this minimizes any overall background to the spectrum. High frequency noise resulting from this double-differentiation is then removed by convolving each spectrum with a $\sigma = 0.38$ meV Gaussian. The lower field spectrum $\rho_1(E)$ is then stretched along the energy axis by a scale factor ϵ and resampled to the same energy resolution as the higher field spectrum $\rho_2(E)$ using linear interpolation. The value of ϵ that maximizes the correlation $\chi(\epsilon) = \int \rho_1(\epsilon E)\rho_2(E)dE$ between the two spectra is then searched for and located. At this point, the best estimate for ϵ is noisy due to discretization of the data in energy. To remove this noise, $\chi(\epsilon)$ is evaluated at 25 values of ϵ over a range stretching from 10% below to 10% above this absolute best correlation, and the resulting curve of χ versus ϵ is fit using a quadratic. The value of ϵ at the peak of this quadratic curve is then selected as the best scale factor for aligning the two spectra at this density.

This process is repeated for every density from $0.1 < \nu < 0.9$ and $1.1 < \nu < 1.9$ in the spectrum. The resulting map of ϵ versus ν is roughly constant; maximum deviations from the mean value are of the order 10%. This flatness indicates that a single value of ϵ is sufficient at all densities to explain the magnetic field dependence of our data. This value is found by averaging the value of ϵ across this range of ν, discarding any outliers that fall more than 3 standard deviations away from the mean. This mean ϵ is used in figure 2**c**. The standard deviation of ϵ across this range of densities is taken as width of the error bars, essentially the range of ϵ found to be a reasonable fit. As such they are not representative of normally distributed statistical errors. However, the reduced sum-squared error (χ^2) still a rough guide as to the quality of different fits. Supplementary Figure 1 shows alternate fits to the B-field dependence.

3 Supplemental Data

Supplementary figure 1 demonstrates that raising the sample temperature to 4.1 Kelvin eliminates the "sash" features while leaving the exchange splitting intact. The broadening of the Fermi function in the tunnel electrode is not sufficient to explain this change. Supplementary Figure 2 demonstrates the insensitivity of the $\nu = 1$ sash to presence of magnetic field in the plane. Supplementary Figure 3 displays the effect of disorder on both the $\nu = 1/2$ sash and the $\nu = 1$ sash. The $\nu = 1/2$ sash is destroyed by disorder in a narrower quantum well whereas the $\nu = 1$ sash survives this disorder.

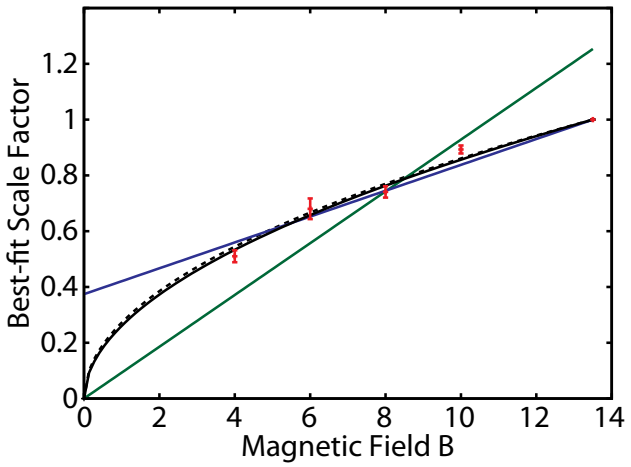

Supplementary Figure 1 | Alternate functional forms for the fit to the magnetic field dependence of the scale factor are less satisfactory than $\sqrt{B}$. Error bars indicate the standard deviation of the scale factor ϵ across the range of available densities at each magnetic field. The fitting functions are $\sqrt{B}$ (solid black line, $\chi^2 = 2.4$), power-law B^α (dotted black line, $\alpha = .52$, $\chi^2 = 3.1$), linear with an offset (blue line, $\chi^2 = 6.9$), and linear without an offset (green line, $\chi^2 = 20$).

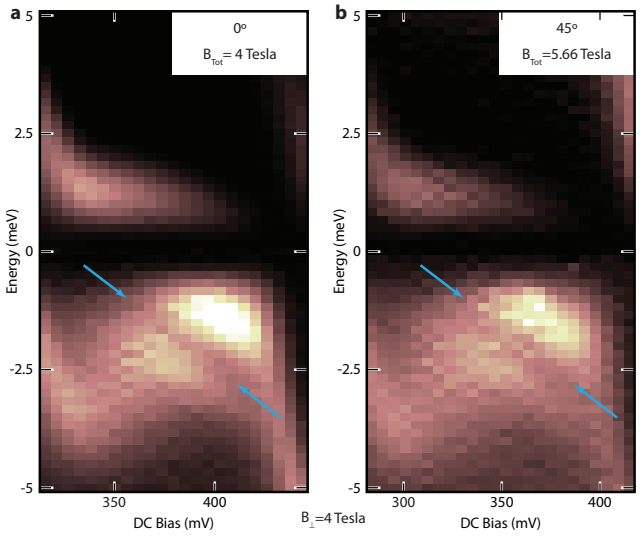

Supplementary Figure 3 | Tilting the sample while maintaining the same magnetic field perpendicular to the quantum well increases the total magnetic field applied. This increases the Zeeman energy (which varies with total field), while keeping the exchange energy (which varies with perpendicular field) fixed. Excitations which originate with the interplay between the Zeeman and exchange energies, including skyrmions, are sensitive to this variation of the total magnetic field. By comparing the spectrum in **b** to **a**, we see that increasing the total magnetic field by 41% does not affect the $\nu = 1$ sash (blue arrows). This data was taken in a device with a 175 Å quantum well at 80 mK.

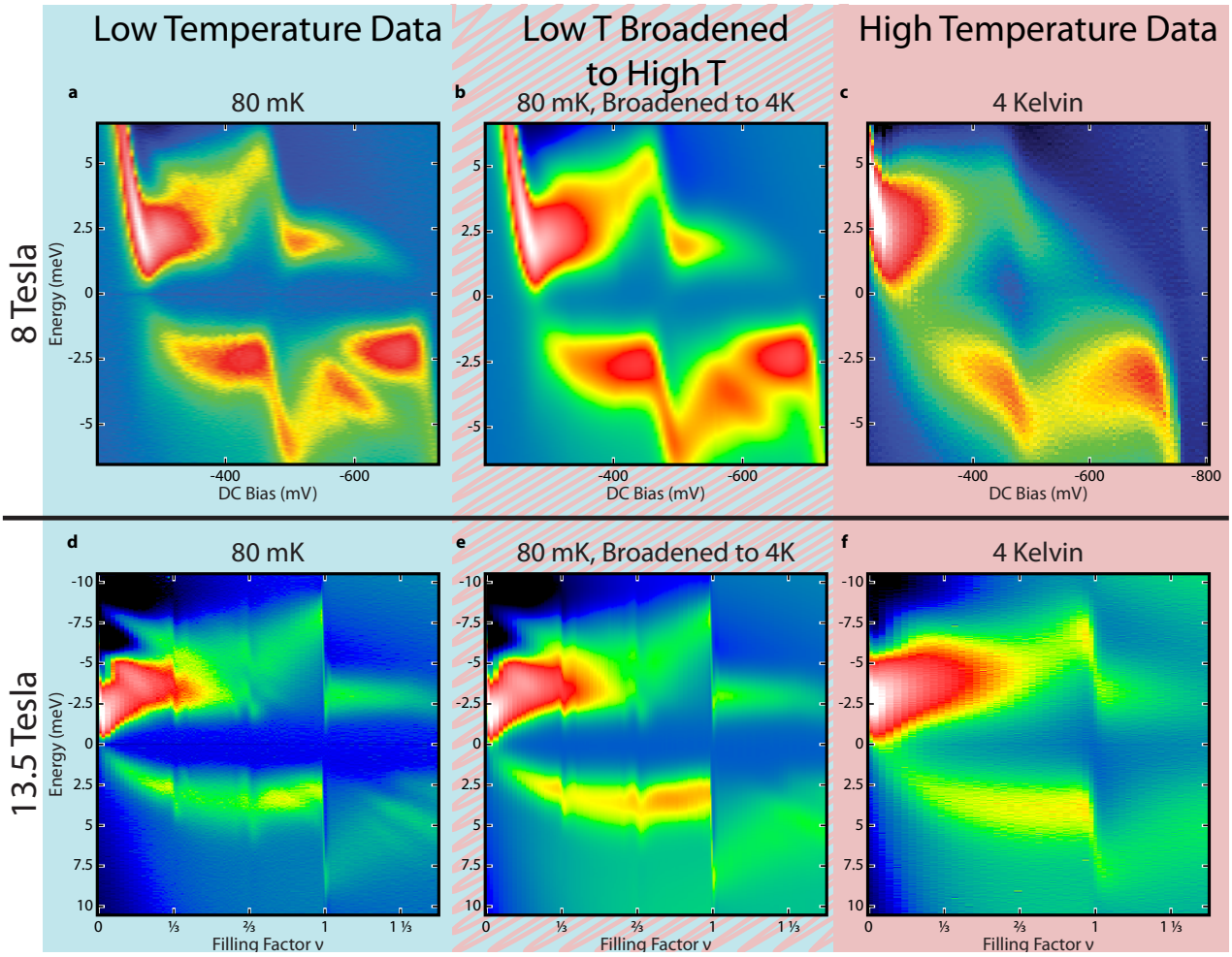

Supplementary Figure 2 | The effect of temperature on the $\nu = 1$ and $\nu = 1/2$ sashes is shown by comparing a spectrum acquired in a 175 Å quantum well at 8 Tesla and 80 mK (**a**) to one measured at 4.1 K (**c**). The effect of Fermi function broadening in the electrode and quantum well can be demonstrated by convolving with a 4.1 K Fermi function (**b**). This does not destroy the sash features, demonstrating that some change in the many-body state of the quantum well is responsible. Similar data at 13.5 Tesla in a 230 Å well also shows the $\nu = 1/2$ sash features completely destroyed at 4.1 Kelvin, while some very slight trace of the $\nu = 1$ sash survives (**d-f**).

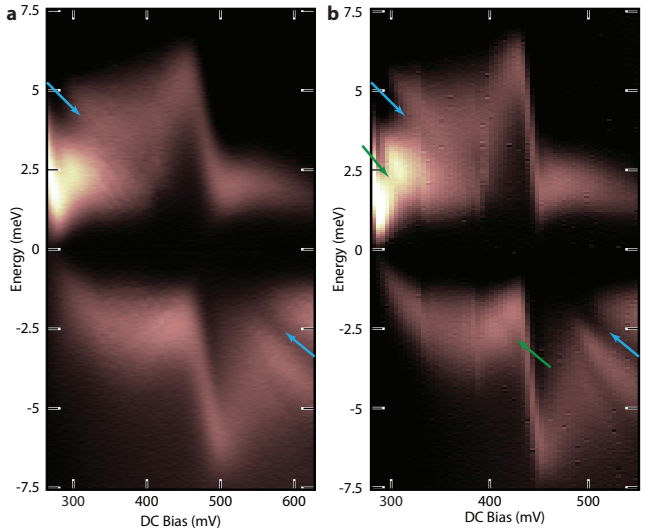

Supplementary Figure 4 | The effect of disorder on the $\nu = 1$ and $\nu = 1/2$ sashes is shown by comparing a spectrum acquired in a 175 Å quantum well (**a**) and a wider 230 Å quantum well (**b**), both with an applied field of 4 Tesla at 80 mK. Although the $\nu = 1$ sash is clearly visible in both spectra (blue arrows), the added disorder from the narrower quantum well almost completely destroys the $\nu = 1/2$ sash (green arrows).

4 Orthogonality Issues in the Composite Fermion Model

Given that whole electrons are tunnelling into the system, not composite particles, why do we observe associated structures in our spectra? Jain has suggested that when the 2DES is in an incompressible fractional state, it may be possible to construct several composite fermions from a whole electron, resulting in a peak in the SPDOS[25;26]. Our peaks sharpen as the 2DES enters fractional Hall plateaus, which we may understand as due to an increase in quasiparticle lifetimes as the system becomes gapped. However, we do not observe any qualitative change in the spectra, nor do we detect a new, sharp resonance. The spectral weight of the peak suggested by Jain may be too small to observe in our otherwise crowded spectra.

Instead, we expect tunnelling directly into a CF Landau level to be strongly suppressed. This suppression reflects the same physics as that responsible for the Coulomb gap at zero energy. In the case of the Coulomb gap, although there is a high thermodynamic density of states at the Fermi energy[27] in a partially filled Landau level, the tunnelling density of states at low energies is reduced by inter-electron repulsion between the tunnelling electron and the electrons already in the quantum well. Similarly, we expect a Coulomb pseudo-gap for tunnelling an electron into a highly correlated CF Landau level. The true energy of the CF level occurs at an energy closer to E_f than the "clouds" of incoherent excitations we observe as the bright part of the "sash"; this is reflected in the placement of the arrows and fans at the edge of the bright part of the sash in the spectra. However, regardless of the exact relationship between the energy of the quasiparticle and the energy of this "cloud", the behaviour of the "cloud" can be used to track the evolution of the quasiparticle as the 2DES density and magnetic field are varied. This measurement is insensitive to quasiparticle charge; when tunnelling an electron into an FQH state with fractional charge $1/q$, conservation of charge demands that we create q excitations, each with energy $\frac{\hbar eB^*}{qm^*}$, requiring a total energy of $\hbar eB^*/m^*$.

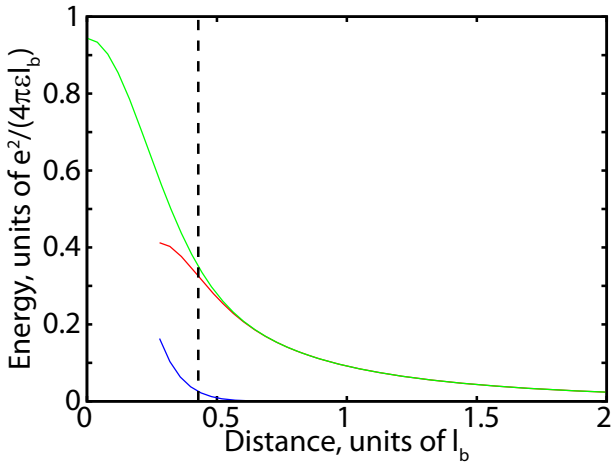

Supplementary Figure 5 | Sample effective potentials calculated for the lattice model show the relatively short range of the exchange attraction. The repulsion between electrons of unlike spins is given by the green curve, while that for like spins by the red curve. The blue line shows the strength of the exchange coupling (the difference between the red and green curves.) Note that the potential for like spins is meaningless at very short distances due to Pauli exclusion. The lattice constant of the hexagonal lattice is shown with the black dotted line.

5 Lattice Model

We use a lattice model based roughly on the one described by Fogler et. al[22]. Each electron is assumed to be localized in a coherent state on a hexagonal lattice. The lattice constant is selected such that one magnetic flux quantum penetrates each unit cell. Periodic boundary conditions are used with a hexagonal lattice, as shown in Supplementary Figure 6**d**. The resulting basis set is almost orthogonal and has the same degeneracy as the true single particle states. Wavefunction overlap is neglected. Electrons of the same spin interact through an effective potential as given by equation 60 of reference 4. However, to address concerns that the spectrum may be modified by the nearby tunneling electrode, the bare Coulomb interaction $v(r)$ is replaced by $\left(e^2/4\pi\epsilon\right)\left(r^{-1}-(r^2+s^2)^{-1/2}\right)$ where s is the distance between the 2D system and the nearby 3D electrode. Electrons of different spins interact through the same potential, but with the exchange term u_{EX} set to zero (Supplementary Figure 5). On each iteration of the software, a single electron is added to the lattice at the most energetically favorable position, and then the electron occupations are selected to minimize the total energy as described in reference 4.

The system is then modified by adding a single electron or hole on one lattice site, and the energy change is calculated and stored. This process is repeated for each possible lattice site, carrier type, and spin. The chemical potential is taken as the mean of the largest hole addition energy and the smallest electron addition energy. The energy difference between the chemical potential and the addition energy is then histogrammed. This histogram is used as an approximation to the SPDOS at this density.

The entire process is then repeated until the lattice is filled, generating a complete simulated TDCS spectrum. The process of filling the lattice is demonstrated in the supplemental movie. Sample results are shown in Supplementary Figure 6. It is worth noting that in the simulations, the nearby electrode does not play a large role once it is more than a magnetic length away. This condition is met in all of the measurements described in this letter. The main role of the screening from this electrode is to diminish distant electron-electron interactions, but the physics of the spectrum is dominated by nearest-neighbor interactions (Supplementary Figure 6**a**,**c**).

The calculated spectra show many "sashes" not present in the experimental spectrum. Although the additional sashes appear to be

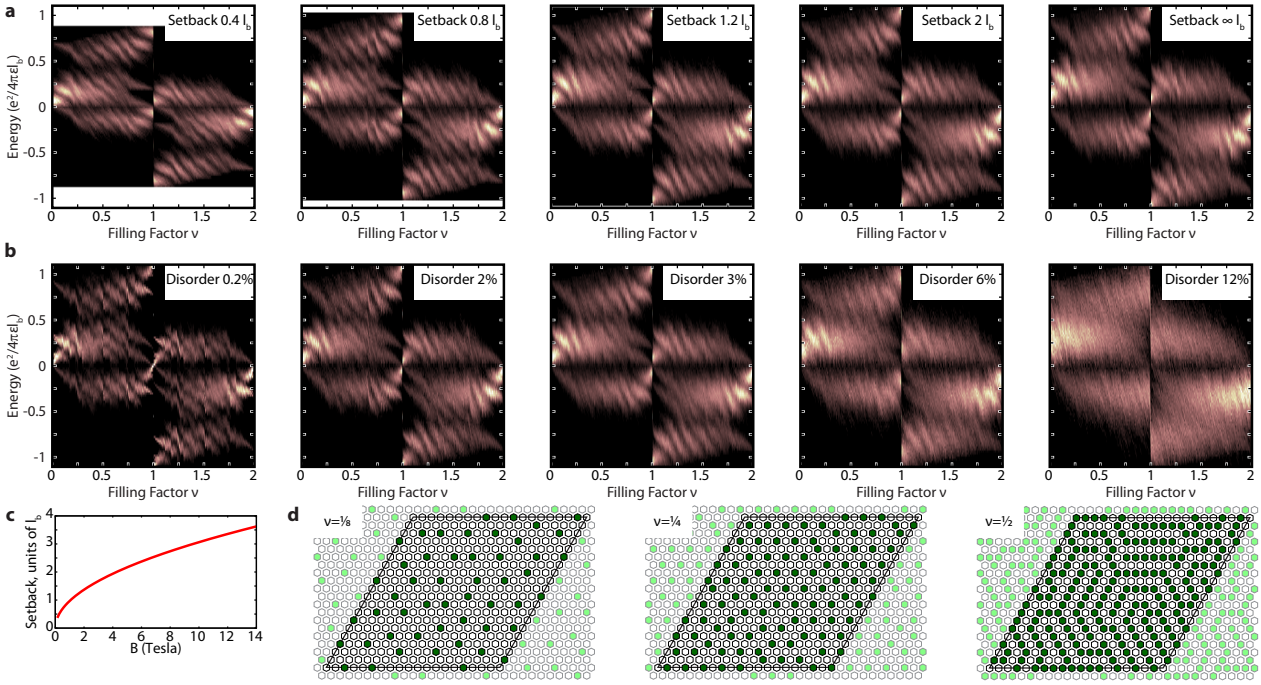

Supplementary Figure 6 | Sample spectra generated by the lattice model exhibit features similar to the experimentally observed sashes. **a** shows a series of simulations with differing setbacks (distances from the center of the quantum well to the 3D electrode) and fixed disorder of 3% of the Coulomb energy scale $e^2/(4\pi\epsilon l_b)$. Note that setbacks of more than l_b have very little impact on the spectrum. The effects of disorder are explored in **b**, where a series of spectra with a fixed setback of 2 l_b but varying disorder, measured as a percentage of the Coulomb energy scale, are shown. The actual setback varies with magnetic field and sample design; the setback appropriate for the device used in these spectra is shown in **c**. Prominent sash features are visible from about 4 to 13.5 Tesla, corresponding to setbacks of 1 to 3 l_b. All spectra are calculated with a 25x25 unit cell. Sample annealed electron lattices are illustrated using a smaller 20x20 unit cell at several filling factors in **d**, with a single unit cell shown in bold. Note the uniformity in the number of occupied neighbor sites. These lattices are for a disorder of 3% and a setback of 2 l_b. See also supplemental movie A.

artifacts of the lattice in our semi-classical model, it is interesting to note that while the addition of disorder diminishes all of the features in the spectrum, these additional sashes appear to diminish more as disorder is increased (see, for example the 6% plot in Supplementary Figure 6**b**). Note that the simulation does not included any lifetime effects. It is not possible to estimate the disorder in our devices from these simulations as it is likely that lifetime broadening influences line-widths in our spectrum and which features are visible in our spectrum.

25. Jain, J. K. & Peterson, M. R. Reconstructing the electron in a fractionalized quantum fluid. *Phys. Rev. Lett.* **94**, 186808 (2005).
26. Vignale, G. Integral charge quasiparticles in a fractional quantum Hall liquid. *Phys. Rev. B* **73**, 073306 (2006).
27. Smith, T. P., Goldberg, B. B., Stiles, P. J. & Heiblum, M. Direct measurement of the density of states of a two-dimensional electron gas. *Phys. Rev. B* **32**, 2696–2699 (1985).